Direct visualization of three-dimensional crystallization behavior in microgels

Melaku Muluneh* and David A. Weitz
Department of Physics, Harvard University, Cambridge, Massachusetts 02138, USA
(Received 8 November 2011; revised manuscript received 27 December 2011; published 10 February 2012)

We use confocal microscopy to study the three-dimensional (3D) structure of colloidal crystals formed by poly(N-isopropylacrylamide)-co-(acrylic acid) microgels of diameter 1.0–1.5 μm. The confocal images are tracked to locate particle positions in 3D, which are used to compute pair-correlation functions $g(r)$, bond order parameters, and structure factors $s(q)$. We find that the structure remains fcc for a range of charge, size, and concentration of the particles. When the particles are weakly attractive and are at low concentrations, polycrystalline solids result. In addition, owing to the compressibility of the colloids, the crystals display remarkable structural stability when subjected to external stress.

DOI: 10.1103/PhysRevE.85.021405 PACS number(s): 82.70.Dd, 61.66.−f, 61.72.−y, 64.70.dg

I. INTRODUCTION

Colloidal modeling of crystallization provides direct and accessible information on the crystallization process in atomic and molecular systems; hard-sphere colloids that interact through volume exclusion are typically used [1–6]. Techniques such as microscopy, rheology, and light scattering are employed to map out the liquid-crystal–amorphous phase transitions in these colloidal suspensions [7–12]. Recently, soft colloids have been used for colloidal crystallization studies owing to their deformability and the ability to use this property as a trigger to induce phase transitions [4,13–19].

A soft colloidal system that is commonly used is a microgel system copolymerized from N-isopropylacrylamide (NIPAm) and acrylic acid (AAc), resulting in poly(N-isopropylacrylamide)-co-(acrylic acid), or p(NIPAm-co-AAc). These microgels have physical and chemical behaviors that are sensitive to pH, ionic strength, temperature, and polymer content [12,20–27]. The ability of the particles to change size as a function of temperature can be used to control volume fraction [14,28]. Compressibility of the particles allows flexibility during crystallization, since softer and bigger particles can shrink to fit into a crystal lattice of smaller and stiffer particles [13]. Microgel suspensions crystallize over a broad range of concentrations due to size changes [16,29]. Simulations have predicted a charge- and size-dependent phase diagram of crystallization [20,30]. Scattering and microscopy experiments in specific instances have found the structures to be fcc [4,16,19]; however, to the best of our knowledge, crystal structures in microgel suspensions consisting of particles of diameter 1.0–1.5 μm as a function of concentration, size, charge, and polymer composition have not been examined. Such a study is thus valuable and contributes to understanding the phase behavior of charged soft colloids.

In this paper, we examine the three-dimensional crystallization behavior in suspensions of p(NIPAm-co-AAc) microgel colloids using confocal microscopy. We use particle-tracking techniques [31] to locate the three-dimensional (3D) positions of the particles in the crystal and subsequently determine the crystal structure by calculating the pair-correlation functions $g(r)$, bond order parameters, and structure factors $s(q)$. Our results show that the crystal structure in these p(NIPAm-co-AAc) suspensions is independent of concentration, charge, size, and stiffness of particles remaining fcc under all conditions. At very low concentrations and at low pH, where crystallization is mainly driven by attraction between particles, the structures formed are polycrystalline solids. We also probe the relationship between compressibility of particles and crystal structure by applying external osmotic pressure on the crystals; the structure stays unchanged, demonstrating that deformability of the colloids enables the suspensions to maintain their crystal structure when subjected to external stress.

II. MATERIALS AND METHODS

We synthesize the microgels through free-radical precipitation copolymerization of NIPAm and AAc, cross-linked with N'-N'-methylene bisacrylamide (BIS), resulting in poly(N-isopropylacrylamide-co-acrylic acid) [32–34]. This yields monodispersed microgels with a fully swollen size in dilute solutions in the range of 1.0–1.5 μm in diameter at 25 °C and 0.3–0.8 μm in diameter above 32 °C as measured by dynamic light scattering [35]. The ratio $D_{\text{swollen}}/D_{\text{collapsed}}$ is thus between 1.2 and 5.0, corresponding to the stiffest and the softest particles, respectively. The ratio of BIS to NIPAm is varied to change the stiffness of particles [36]. Rhodamine B (PolyFluor 570) is used for fluorescent labeling. The particles are cleaned by repeated centrifugation and redispersion in de-ionized water. A series of concentrations are then prepared by dispersing the concentrated suspension in solutions whose pH values are adjusted using 0.1M HCl. The change in pH translates into a change of charge on the particles. This is verified by measuring the zeta potential of the particles (Malvern Zetasizer), found to be −0.7 mV at pH = 3.0, −12 mV at pH = 5.0, and −16 mV at pH = 7.0. These agree with values given elsewhere [37]. The charge is then deduced as described previously [38,39]. We find that particles have a net charge of ∼60e at pH = 3.0, ∼3000e at pH = 5.0, and ∼4000e at pH = 7.0, respectively, where e is the electron charge.

Each sample is initialized by applying shear on a vortexer for 3 min. The sheared sample is placed in an imaging cell, and left to equilibrate for 3 days at room temperature. This ensures that there is enough time for samples at low

*mmuluneh@fas.harvard.edu

concentrations to complete the crystallization process. Images are recorded with a confocal microscope (Leica SP5) equipped with a 100 × numerical aperture (NA) 1.4 oil immersion objective [40,41]. This allows us to directly visualize the suspension deep into the bulk of our sample and still obtain high-quality images; microgels are inherently close to index matched since the particles themselves typically contain more than 90% of solvent. The temperature of the samples is kept at 25 °C by using objective warmers fitted on the microscope (Warner Instruments) in a room maintained at a slightly lower temperature. The 3D field of view for our image stacks is 35 × 35 × 10 μm^3, containing between 5000 and 15 000 particles. Images are recorded at a distance of ∼5 particle diameters away from the bottom coverslip and several micrometers away from the side walls to minimize wall effects [42,43]. Ten image stacks are acquired from separate locations of the sample cell. After image acquisition, the particle positions are determined using particle tracking algorithms [31].

Microgel particles shrink when the concentration of the suspension increases; we therefore define an effective volume fraction of particles as $\zeta = V_o n$, where V_o is the volume of a particle in dilute suspension, and n is the number density of particles [12,24]. Measurement of the hydrodynamic radius is complicated by the polymer-brush extensions on the particles which have the effect of enlarging the value; as a result, a direct parallel between ζ and the colloidal volume fraction is not straightforward. At higher concentrations when the particles become compressed, ζ can reach values much larger than unity. ζ is used to provide a self-consistent calibration for a sample with a given cross-linker-to-monomer ratio and should not be compared to the traditional colloidal volume fraction. Cross-comparing values from different samples is also not useful since the particle structure, pH, and a slight variation in synthesis can introduce changes from sample to sample, making such a comparison arbitrary. Nevertheless, we see phase transitions to occur for values of ζ within a range of five percentage points; for example, crystallization of samples starts when $\zeta = 0.55 \pm 0.05$. The parameter also provides information on the range of concentrations over which crystallization occurs for a specific sample, and allows us to roughly compare the trend between ranges of concentrations of different samples.

III. RESULTS AND DISCUSSION

Microgels crystallize over a broad range of concentrations [16]. Crystallization is facilitated by the ability of the particles to shrink, as this minimizes the effect of any polydispersity [13,16], a key behavior that differentiates microgels from hard-sphere colloidal systems. Figure 1 shows a sequence of two-dimensional (2D) images of microgel crystals for the cross-linker-to-monomer ratio, BIS:NIPAm (or b:n from here on), of 8% at concentrations of $\zeta = 0.84$, 0.94, 1.73, and 1.86, respectively. The higher the concentration, the smaller is the size of the particles and the distances between them, illustrating the deswelling behavior of these colloids [12], a characteristic that makes it possible for the suspensions to crystallize over a broad range of concentrations.

The crystal structure is analyzed by calculating the pair-correlation function $g(r)$, which measures the probability

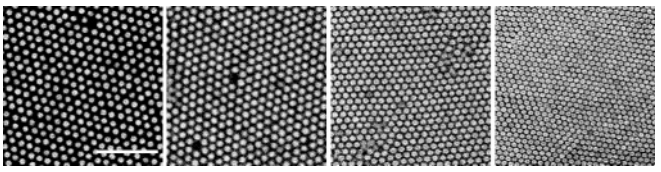

FIG. 1. Size change with concentration in microgel crystals. xy images taken parallel to the bottom coverslip of crystals at $\zeta = 0.84$, 0.94, 1.73, and 1.86 for a sample with 8% b:n (bis:nipam). The scale bar is 8 μm.

of finding a particle a distance r from a particle at the center. For a perfect crystalline system, $g(r)$ is characterized by peaks at well-defined values. For example, an ideal fcc crystal structure has $g(r)$ peaks at r/α values of $\sqrt{1}$, $\sqrt{2}$, $\sqrt{3}$, $\sqrt{4}, \ldots$, where α is the position of the first peak [44]. The $g(r)$ peak positions from the microgel crystals are then used to determine the structure. In Fig. 2, we have plotted the $g(r)$ for samples with different b:n, pH, and ζ. The horizontal axis is normalized by the first peak position of $g(r)$, α. The plots for each concentration are offset vertically for clarity. The dashed vertical lines represent the theoretical peak positions for an ideal fcc stacking. In the insets are the crystal bond order parameters Q_6 and W_6 [45]. The results obtained for $g(r)$ and order parameters across the different cross-linker-to-monomer ratios and different concentrations agree with theoretical values for fcc stacking. This uniformity in the results obtained across samples of different stiffnesses confirm that changes in the internal structure of the particles due to the variation of cross-linker-to-monomer ratio [23,46] do not play a role in determining how these particles arrange in crystals. Moreover, the fcc stacking structure of crystals in these systems is independent of colloid concentration.

In addition to the concentration and particle internal structure, the charge on the particles may change the phase behavior of these suspensions by influencing the electrostatic interactions between the particles [47–49]. The amount of charge on the particles can be controlled by changing the pH of the suspensions, as confirmed by our zeta potential measurements. At low pH, it is possible that the carboxylic groups of AAc are mostly protonated, making the particles less charged; it is thus likely that hydrogen bonding overcomes charge repulsion to cause attraction between particles [17,22]. By contrast, at high pH, particles are more charged and, as a result, are repulsive. The results in Fig. 2 are obtained at three different pH levels. The peaks in the $g(r)$ reveal that the structures both in the attractive and repulsive conditions are in agreement with predictions for fcc stacking. Simulation results have predicted a charge-dependent crystal structure for ionic microgels of diameter 0.1–0.5 μm and of charge of less than 600e [20,30]; some agreement of the theory with experiment has been reported [50]. Although a direct comparison between our data and the theory cannot be made, we see no evidence of the variation of structure with charge or concentration in our microgel suspensions.

To investigate spatial order, we look at the structure factor $s(q)$ of the crystals [2,51]. Figure 3(a) shows a 2D image of a crystal plane for the 8% b:n sample at pH = 7.0 and ζ = 0.84; the particles in the image are arranged hexagonally, as confirmed by its Fourier transform that contains hexagonal

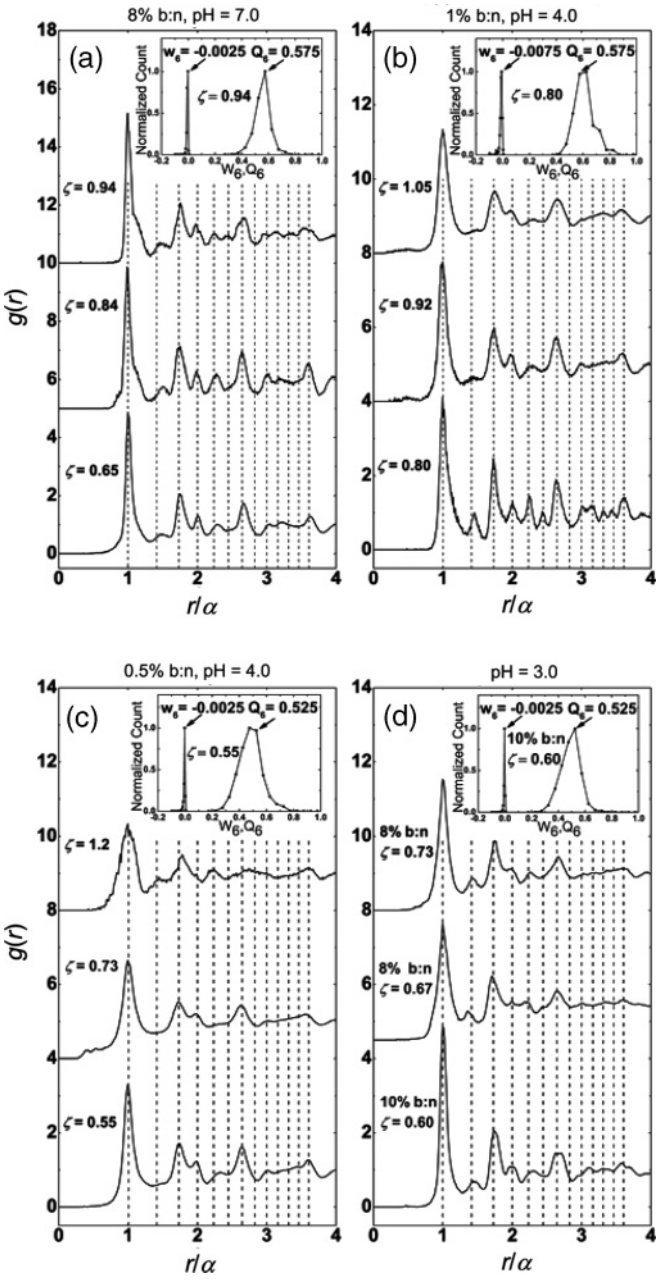

FIG. 2. Pair-correlation functions for various samples at different concentrations and pH values show agreement with the fcc crystal structure throughout. The data shown here are for samples with bis:nipam (b:n) of (a) 8% at $p\mathrm{H} = 7.0$ for $\zeta = 0.65$, 0.84, and 0.94, (b) 1% at $p\mathrm{H} = 4.0$, for $\zeta = 0.84$, 0.92, and 1.05, (c) 0.5% at $p\mathrm{H} = 4.0$, for $\zeta = 0.55$, 0.73, and 1.2, and (d) 8.0% at $p\mathrm{H} = 3.0$, $\zeta = 0.67$, 0.73 and 10% at $p\mathrm{H} = 3.0$, $\zeta = 0.60$. In the insets are the bond order parameters Q_6 and W_6 for representative samples: (a) 8% b:n at $p\mathrm{H} = 7.0$, $\zeta = 0.94$. (b) 1% b:n at $p\mathrm{H} = 7.0$, $\zeta = 0.84$. (c) 0.5% b:n at $p\mathrm{H} = 4.0$, $\zeta = 0.55$. (d) 10% b:n at $p\mathrm{H} = 3.0$, $\zeta = 0.60$.

points similar to Fig. 3(b). The peaks in $s(q)$ are nodes arranged hexagonally, as expected for an extended crystal in 3D [Fig. 3(b)]; the highly localized nature of the nodes in reciprocal space means there is both translational and orientational order in the crystal [2,51].

For further analysis of stacking in 3D, we render the crystals as shown in Fig. 3(c), where four layers of the 111 planes are

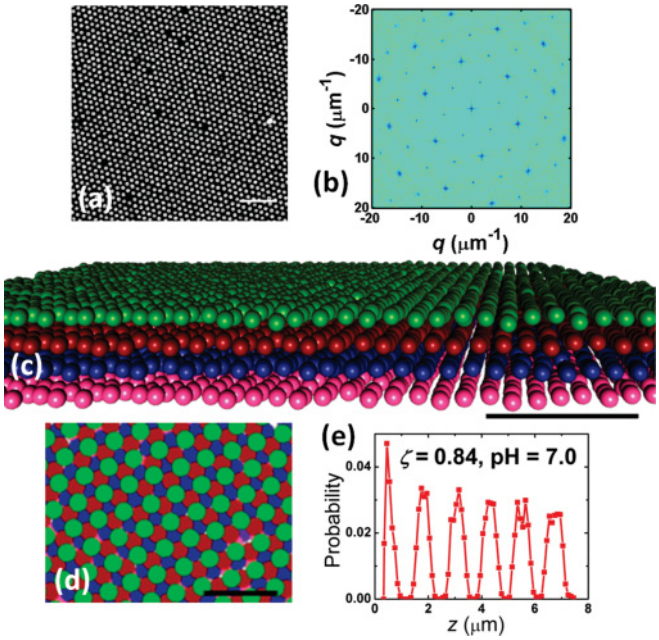

FIG. 3. (Color online) Crystal features of a sample with 8% b:n at $p\mathrm{H} = 7.0$ for $\zeta = 0.84$. (a) A confocal xy image taken parallel to the bottom coverslip. The scale bar is 8 μm. (b) A 2D $s(q)$ of the 3D stack. (c) A side view of a rendering in 3D. The scale bar is 8 μm. (d) A top view of the rendering in (c). The scale bar is 4 μm. (e) Probability distribution of the particle distance from bottom cover slip.

reconstructed from the tracked data. An ABCABC. . . stacking of such planes is indicative of fcc crystal structure [2,6]. The arrangement of the planes is ABCA, with the bottom and top layers aligned. Looking at the rendered data perpendicular to the 111 planes as shown in Fig. 3(d) clearly shows the three layers at locations displaced with respect to each other as expected. The particles are arranged parallel to the bottom coverslip [Figs. 3(c) and 3(e)]. In Fig. 3(e), the probability distribution of the z position is plotted as a function of height from the bottom coverslip, showing nonzero probabilities only at the location of the horizontal planes, illustrating the highly ordered nature of the stacking. The stacking of horizontal planes can extend tens of micrometers above the bottom coverslip.

Microgels at low pH crystallize at lower concentrations due to attraction between the particles [12,16,17,29] even though the suspensions are not sufficiently crowded to form crystals through entropic forces. Looking at the spatial profile of the crystals helps to understand how this occurs. At high pH and when particles are repulsive, the structures are mainly extended single crystals that cover the full field of view as in Fig. 4(a). By contrast, at low pH, defects and dislocations become more common [Fig. 4(b)], and at low concentration, a polycrystalline structure results [Fig. 4(c)]. Nevertheless, the peaks in the $g(r)$ still agree with the expected values for fcc structure [Fig. 2(d)]. The change in the size of the crystals is also reflected in the broadening of the peaks in $s(q)$. The hexagonal sharp nodes that characterize extended single crystals [Fig. 4(d)] now become broader and also get

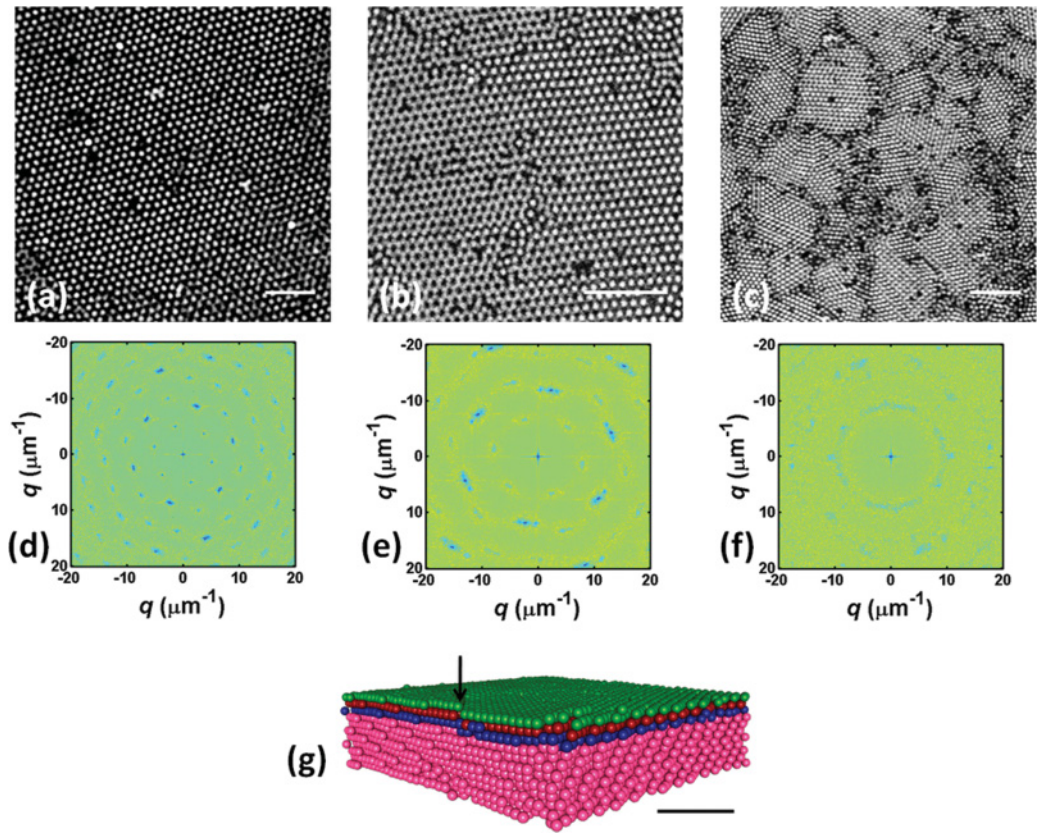

FIG. 4. (Color online) Spatial structure of samples with 8% b:n. The scale bars are 8 μm. Top row: xy images of samples for (a) $\zeta = 0.65$ and pH $= 7.0$, (b) $\zeta = 0.73$ and pH $= 3.0$, and (c) $\zeta = 0.67$ and pH $= 3.0$. The corresponding $s(q)$ of each are shown in (d), (e), and (f), respectively. (g) 3D rendering of the sample in (b). The black arrow shows the line of dislocation.

weaker at higher-order reflections [Figs. 4(e)–4(f)]. Nearly half of the particles in Fig. 4(b) are out of focus owing to a dislocation perpendicular to the bottom coverslip. The rendering in Fig. 4(g) shows how multiple layers of the stacking are displaced in the vertical direction; the black arrow indicates where this has occurred. Such defects are introduced when crystallization occurs due to attraction even though the concentration is too low for crystals to form entropically.

Spontaneous crystallization does not occur above $\zeta = 0.94$, 1.05, and 1.2 for 8%, 1%, and 0.5% b:n, respectively. Beyond these concentrations, the suspensions stay amorphous even after a few weeks. To further investigate the effect of deformability on the structure and stability of the crystals formed, we subject the crystallized suspensions to an external osmotic pressure. A 10-wt % Dextran ($M_r \sim 70$ k/mol) solution is used to apply osmotic pressure of about 20 kPa [52] to a crystallized sample, as shown in the schematic in Fig. 5(a). Figure 5(b) shows the $g(r)$ for the sample with 8% b:n at neutral pH which is concentrated to $\zeta = 1.73$ by applying the external osmotic pressure for 2 h; the fcc peaks are still prominent, illustrating the ability of the suspension to maintain the overall structure while individual particles shrink in size. The fcc peaks tend to remain in place even after the system has been subjected to osmotic pressure for 12 h [Fig. 5(b)] and when the concentration has reached $\zeta = 1.86$. The $s(q)$ is still characterized by hexagonal nodes for the sample at $\zeta = 1.73$; this shows the persistence of spatial order in the resulting crystal [Fig. 5(c)].

IV. CONCLUSION

Microgel suspensions consisting of particles of diameter 1.0–1.5 μm are allowed to crystallize spontaneously over 3 days for different particle charges, concentrations, and stiffnesses, and are imaged under a confocal microscope to determine the crystal structure. The tracked particle positions are used to calculate the pair-correlation functions, bond order parameters, and structure factors. Results obtained for $g(r)$ and bond order parameters agree with those predicted for fcc crystal structure at all particle concentrations and stiffnesses. In addition, the results do not depend on the charge on the particles, as demonstrated by experiments done by varying the pH of the suspensions. At neutral pH where the particles are repulsive [22] and crystallization is driven by entropic forces, the crystals have both translational and orientational order, as shown by the hexagonal sharp nodes in the structure factor. At low pH and low concentration where crystallization is not entropically driven and is the result of attraction-induced nucleation [12], the resulting structures are polycrystalline. The ability of the particles to shrink by expelling solvent during either gravitational or osmotic pressure means that they can be made to pack to high concentrations with $\zeta > 1.0$. Spontaneous crystallization ceases to occur past a critical

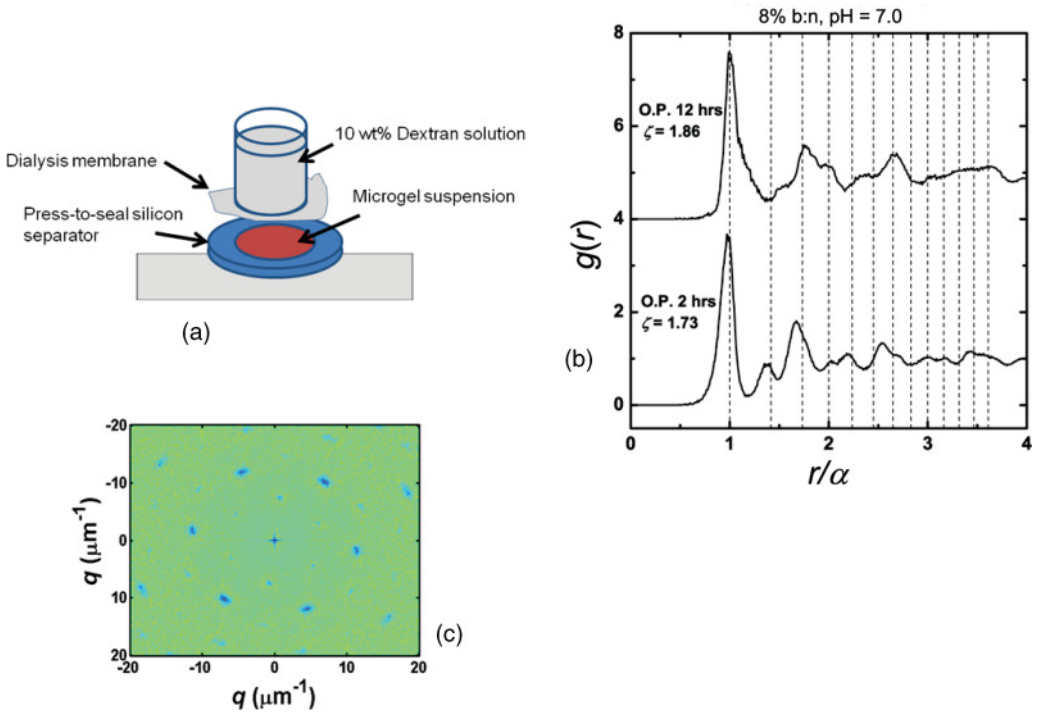

FIG. 5. (Color online) Osmotic pressure (OP) applied to a sample with 8% b:n at pH = 7.0 and the resulting structure. (a) A sketch of the experimental setup. (b) The resulting $g(r)$ of samples for which the OP is applied for 2 h (bottom graph) and 12 h (top graph) with final $\zeta =$ 1.73 and 1.86, respectively. (c) $s(q)$ of a sample with $\zeta = 1.73$.

concentration; nevertheless, crystals at higher than this critical concentration can be obtained by applying external osmotic pressure to already crystallized samples. Surprisingly, the crystal structures before and after the application of external osmotic pressure are identical, illustrating the remarkable ability of the suspensions to neutralize external stress, a unique feature of these soft spheres.

ACKNOWLEDGMENTS

We thank Joris Sprakel for help with $s(q)$ analysis. We thank Erick Weeks and John Crocker for the use of their particle tracking algorithms. This work was supported by the Harvard MRSEC (DMR-0820484), and the NSF (DMR-1006546).

[1] U. Gasser, A. Schofield, and D. A. Weitz, J. Phys. Condens. Matter **15**, S375 (2002).
[2] J. Liu, D. A. Weitz, and B. J. Ackerson, Phys. Rev. E **48**, 1106 (1993).
[3] U. Gasser, E. R. Weeks, A. Schofield, P. N. Pusey, and D. A. Weitz, Science **292**, 258 (2001).
[4] A. M. Alsayed, M. F. Islam, J. Zhang, P. J. Collings, and A. G. Yodh, Science **309**, 1207 (2005).
[5] P. Schall, I. Cohen, D. A. Weitz, and F. Spaepen, Science **305**, 1944 (2004).
[6] P. N. Pusey, W. v. Megen, P. Bartlett, B. J. Ackerson, J. G. Rarity, and S. M. Underwood, Phys. Rev. Lett. **63**, 2753 (1989).
[7] C. Allain, M. Cloitre, and M. Wafra, Phys. Rev. Lett. **74**, 1478 (1995).
[8] J. L. Harland, and W. v. Megen, Phys. Rev. E **55**, 3054 (1997).
[9] W. v. Megen, and P. N. Pusey, Phys. Rev. A **43**, 5429 (1991).
[10] H. J. Schope, G. Bryant, and W. v. Megen, Phys. Rev. Lett. **96**, 175701 (2006).
[11] W. v. Megen, and S. M. Underwood, Phys. Rev. E **49**, 4206 (1994).
[12] M. Muluneh, J. Sprakel, H. Wyss, J. Mattsson, and D. Weitz, J. Phys. Condens. Matter **23**, 505101 (2011).
[13] A. S. J. Iyer and L. A. Lyon, Angew. Chem., Int. Ed. **48**, 4562 (2009).
[14] Y. Han, N. Y. Ha, A. M. Alsayed, and A. G. Yodh, Phys. Rev. E **77**, 41406 (2008).
[15] Z. Hu and G. Huang, Angewandte Chemie **115**, 4947 (2003).
[16] L. A. Lyon, J. D. Debord, S. B. Debord, C. D. Jones, J. G. McGrath, and M. J. Serpe, J. Phys. Chem. B **108**, 19099 (2004).
[17] Z. Meng, J. K. Cho, S. Debord, V. Breedveld, and L. A. Lyon, J. Phys. Chem. B **111**, 6992 (2007).
[18] D. Suzuki, J. G. McGrath, H. Kawaguchi, and L. A. Lyon, J. Phys. Chem. C**111**, 5667 (2007).
[19] T. Hellweg, C. D. Dewhurst, E. Bruckner, K. Kratz, and W. Eimer, Colloid Polym. Sci. **278**, 972 (2000).
[20] D. Gottwald, C. N. Likos, G. Kahl, and H. Lowen, Phys. Rev. Lett. **92**, 068301 (2004).
[21] A. Fernandez-Nieves, A. Fernandez-Barbero, B. Vincent, and F. J. d. l. Nieves, J. Chem. Phys. **119**, 10383 (2003).

[22] J. K. Cho, Z. Meng, L. A. Lyon, and V. Breedveld, Soft Matter **5**, 3599 (2009).
[23] T. G. Mason and M. Y. Lin, Phys. Rev. E **71**, 040801 (2005).
[24] J. Mattsson, H. M. Wyss, A. Fernandez-Nieves, K. Miyazaki, Z. Hu, D. R. Reichman, and D. A. Weitz, Nature **462**, 83 (2009).
[25] H. Senff and W. Richtering, Colloid Polym. Sci. **278**, 830 (2000).
[26] J. Wu, B. Zhou, and Z. Hu, Phys. Rev. Lett. **90**, 048304 (2003).
[27] M. J. Snowden, B. Z. Chowdhry, B. Vincent, and G. E. Morris, J. Chem. Soc., Faraday Trans. **92**, 5013 (1996).
[28] S. Tang, Z. Hu, Z. Cheng, and J. Wu, Langmuir **20**, 8858 (2004).
[29] S. B. Debord and L. A. Lyon, J. Phys. Chem. B **107**, 2927 (2003).
[30] D. Gottwald, C. N. Likos, G. Kahl, and H. Lowen, J. Chem. Phys. **122**, 074903 (2005).
[31] J. C. Crocker and D. G. Grier, J. Colloid Interface Sci. **179**, 298 (1996).
[32] X. Wu, R. H. Pelton, A. E. Hamielec, D. R. Woods, and W. McPhee, Colloid Polym. Sci. **272**, 467 (1994).
[33] R. Pelton, Adv. Colloid Interface Sci. **85**, 1 (2000).
[34] D. Duracher, A. Elaissari, and C. Pichot, J. Polym. Sci., Part A: Polym. Chem. **37**, 1823 (1999).
[35] J. K. G. Dhont, in *An Introduction to Dynamics of Colloids* (Elsevier, Amsterdam, 1996), p. 107.
[36] B. Sierra-martin, J. A. Frederick, Y. Laporte, G. Markou, J. J. Leitor-Santos, and A. Fernandez-Nieves, Colloid Polym. Sci. **289**, 721 (2011).
[37] S. Schmidt, T. Hellweg, and R. v. Klitzing, Langmuir **24**, 12595 (2008).
[38] H. Ohshima, T. W. Healy, and L. R. White, J. Colloid Interface Sci. **90**, 17 (1982).
[39] D. W. Schaefer, J. Chem. Phys. **66**, 3980 (1977).
[40] A. D. Dinsmore, E. R. Weeks, V. Prasad, A. C. Levitt, and D. A. Weitz, Appl. Opt. **40**, 4152 (2001).
[41] P. J. Lu, P. A. Sims, H. Oki, J. B. Macarthur, and D. A. Weitz, Opt. Express **15**, 8702 (2007).
[42] P. Wette, A. Engelbrecht, R. Salh, I. Klassen, D. Menke, D. M. Herlach, S. V. Roth, and H. J. Schope, J. Phys. Condens. Matter **21**, 464115 (2009).
[43] M. Franke, A. Lederer, and H. J. Schope, Soft Matter **7**, 11267 (2011).
[44] M. Parrinello and A. Rahman, Phys. Rev. Lett. **45**, 1196 (1980).
[45] P. J. Steinhardt, D. R. Nelson, and M. Ronchetti, Phys. Rev. B **28**, 784 (1983).
[46] M. Stieger, W. Richtering, J. S. Pedersen, and P. Linder, J. Chem. Phys. **120**, 6197 (2004).
[47] A. N. S. John, V. Breedveld, and L. A. Lyon, J. Phys. Chem. B **111**, 7796 (2007).
[48] Z. Meng, J. K. Cho, V. Breedveld, and L. A. Lyon, J. Phys. Chem. B **113**, 4590 (2009).
[49] A. R. Denton, Phys. Rev. E **67**, 011804 (2003).
[50] P. S. Mohanty and W. Richtering, J. Phys. Chem. B **112**, 14692 (2008).
[51] P. M. Chaikin, and T. C. Lubensky, in *Principles of Condensed Matter Physics* (Cambridge University Press, Cambridge, 1997), p. 30.
[52] Y. D. Livney, O. Ramon, E. Kesselman, U. Cogan, S. Mizrahi, and Y. Cohen, J. Polym. Sci., Part B: Polym. Phys. **39**, 2740 (2001).